IEEE Access
Multidisciplinary ⋮ Rapid Review ⋮ Open Access Journal

Received September 28, 2020, accepted October 30, 2020, date of publication November 20, 2020,
date of current version December 8, 2020.

Digital Object Identifier 10.1109/ACCESS.2020.3039629

Unbalanced Magnetic Pull Effects on Rotordynamics of a High-Speed Induction Generator Supported by Active Magnetic Bearings – Analysis and Experimental Verification

HEESOO KIM[1], EERIK SIKANEN[1], JANNE NERG[2], (Senior Member, IEEE), TEEMU SILLANPÄÄ[2], (Member, IEEE), AND JUSSI T. SOPANEN[1], (Member, IEEE)

[1]Department of Mechanical Engineering, LUT University, 53850 Lappeenranta, Finland
[2]Department of Electrical Engineering, LUT University, 53850 Lappeenranta, Finland

Corresponding author: Heesoo Kim (heesoo.kim@lut.fi)

This work was supported by funding from the LUT Doctoral School, TEKES-the Finnish Funding Agency for Technology and Innovation under grant 2748/31/2013, and South Carelian Regional Fund under grant AIKOKASVU EK15.

ABSTRACT Unbalanced magnetic pull (UMP) resulting from air-gap eccentricity can present a potential risk to the lifetime and dynamic stability of high-speed electrical machines. Nevertheless, a method to identify the effects of UMP in actual industrial machines has not yet been sufficiently developed. In this paper, methods for analysis and experimental verification of UMP effects are studied using a high-speed two-pole induction generator supported by active magnetic bearings (AMBs) as a case example. The UMP force is calculated using a semi-analytical model that combines an analytical model with a correction factor obtained from finite element analysis (FEA) results. Using this model, the characteristics of time-variant UMP that are related to the effects of UMP on rotordynamics are investigated. Coefficients for the rotor–bearing simulation model are identified using a detailed CAD model and experimental modal analysis data. Linearized coefficients of AMBs are identified based on the rigid body whirling mode of the rotor. Then, UMP effects are investigated by conducting a time-step rotordynamic simulation in the mixed eccentricity condition, and the results are verified by comparing them with the vibration measurement results during ramp-down operation of the test machine. Results show two main effects produced by UMP on the rotordynamics of induction machines, namely reduction in the rotor natural frequency and additional vibration caused by twice the supply frequency excitation, thus confirming that the proposed semi-analytical UMP model is suitable for the rotordynamics simulation and achieves a high accuracy with efficient computation.

INDEX TERMS Active magnetic bearings, air-gap eccentricity, electromagnetic forces, induction motors, rotordynamics, unbalanced magnetic pull, vibrations.

I. INTRODUCTION

Demand for high-speed electrical machines is continuously increasing because of their recognized advantages, such as high efficiency and possibility of direct connection with working machines. At the same time, technological problems, such as high mechanical stresses in the rotor material, noise, and vibration, and challenges of high-frequency controller design, have emerged. From the viewpoint of rotordynamics, high vibration is an important issue to be tackled as it can shorten the lifetime of the machine. Unbalanced magnetic pull (UMP) is known to increase vibration in electrical machines, but it has not yet been sufficiently studied to accurately simulate the effect and identify it with experimental results. Specifically, in the case of an induction machine, which is the most common electrical machine type applied in industry, it is difficult to estimate UMP, because in a machine of this type, the effect of rotor current has to be considered. This paper focuses on the study of UMP in an induction machine.

The associate editor coordinating the review of this manuscript and approving it for publication was Pinjia Zhang.

To study the rotordynamic effect of UMP, an accurate and computationally efficient UMP force model is needed. The UMP calculation methods can be divided into three categories: analytical and numerical methods, and a combination of these two [1]. A commonly used process is to obtain the asymmetric air-gap magnetic flux density distribution and then calculate the UMP force by using the Maxwell stress method. For this purpose, it is important to solve the magnetic field in the eccentric condition. Dorrell *et al.* [2] obtained the air-gap magnetic flux density by calculating both the stator MMF and the rotor MMF from the induced rotor electromotive force (EMF) in induction machines with a squirrel cage rotor. Chuan *et al.* [3] introduced the UMP damping coefficient for considering the effect of the counteracting flux produced by a parallel-connected cage rotor and proposed an empirical method to calculate the UMP. In this method, finite element analysis (FEA) or experimental results were used to determine the parameters in the UMP equation. Holopainen *et al.* [4] developed an electromechanical rotor model including the UMP force for a rotor moving in an arbitrary orbit without any predefined eccentricity condition in cage induction motors. The parameters in the model were estimated by using an impulse method based on FEA. Kim *et al.* [5], [6] developed a rotordynamics simulation method based on a mixed rotor eccentricity model for time-step analysis in an induction motor. They proposed an optimal way to calculate the UMP force by using a simple analytical model and its update with FEA.

For the verification of the analytical UMP model, several attempts to measure UMP force experimentally have been reported in the literature. Dorrell *et al.* [7] and Zhu *et al.* [8] designed specific test rigs to measure the UMP force under variation in air-gap eccentricity in the cases of an induction machine and a permanent magnet brushless machine. In these test rigs, arbitrary air-gap eccentricity was produced by controlling the location of the stator or rotor accurately by using a three-axis movement support with a load cell that measures the UMP force. Arkkio *et al.* [9] measured the UMP force in a test machine (induction motor) equipped with active magnetic bearings (AMBs). In their test rig, the AMB system generated eccentric rotor motion as an exciter and measured the UMP force by a force sensor.

Further attempts to determine the UMP effect on rotordynamics experimentally have been reported in the literature. For instance, Pennacchi [10] evaluated the UMP effect by investigating the vibrational behavior of a steam turbogenerator and comparing the results between no-load and load conditions of the generator. Kim *et al.* [5] produced the static eccentricity condition by installing a shim on one side between the motor frame and the bearing housing. Then, they measured the vibration of the motor frame in the conditions of different static eccentricities, and the effect of UMP was investigated. According to previous studies, it is a challenging task to control the air-gap eccentric condition in an actual rotating machine. As a solution to this problem, a machine supported by AMBs is a viable option for experimental study, because AMBs can control the rotor center, in other words, variable static eccentricity conditions can be achieved by AMBs.

The objective of this study is to simulate the effect of UMP in an actual industrial induction machine accurately and efficiently by using a previously studied semi-analytical UMP model [6], and then verify the results experimentally. Specifically, the study focuses on a method to verify the UMP effect on rotordynamics rather than the UMP force itself because the vibrational effect of the UMP is directly related to the rotordynamics of the machine. As the literature survey of previous experimental studies shows, it is, however, a challenging task to demonstrate the air-gap eccentricity condition without building a specific test rig. Therefore, it is valuable and motivated to develop a solution to measure the UMP effect using only existing equipment in the system without any modifications. The solution is feasible in an application supported by AMBs because of their integrated system for rotor control and displacement measurement. Therefore, in this study, an industrial-scale prototype of a steam turbogenerator supported by AMBs is selected as the test machine, and an experimental verification process that can be applied to actual industrial machines is proposed to determine UMP effects on rotordynamics. Finally, the UMP effect is determined by comparing simulation and experimental results. Moreover, the cause of the UMP effects is interpreted using the characteristics of the UMP force and stiffness analyzed in this paper.

II. UMP MODEL FOR ROTORDYNAMICS SIMULATION

In this section, the UMP model for rotordynamics simulation is introduced in brief; more details of the model can be found in a previous study [6]. First, mixed eccentricity is modeled based on dynamic motion of the rotor and the concept of time-step simulation. Then, the UMP force and stiffness are modeled with a semi-analytical method by using a simple analytical equation and FEA calculation results to improve the accuracy of the analytical model.

A. MIXED ROTOR ECCENTRICITY MODEL

To simulate the actual condition of the rotor eccentricity, the eccentricity model must consider both the static and dynamic eccentricities simultaneously (mixed eccentricity). Fig. 1 shows the concept of the developed mixed eccentricity model. In this model, the instantaneous position of the rotor center is determined from the time-variant rotor whirling motion, which is defined in the x_2-y_2 coordinate system parallelly translated from the stator reference coordinate system (x_1-y_1) with the amplitude and direction angle of the static eccentricity. Here, the whirling motion of the rotor can be expressed by using time-dependent dynamic eccentricity terms. Then, mixed eccentricity is defined in the stator reference coordinate frame by using static eccentricity and dynamic eccentricity terms. The amplitude and direction

angle of the mixed eccentricity are expressed as

$$e_{\mathrm{mix}}(t) = \sqrt{\begin{array}{l}\left(e_{\mathrm{st}}\cos\theta_{\mathrm{st}} + e_{\mathrm{dy}}(t)\cos\left(\theta_{\mathrm{dy}}(t)\right)\right)^2 \\ +\left(e_{\mathrm{st}}\sin\theta_{\mathrm{st}} + e_{\mathrm{dy}}(t)\sin\left(\theta_{\mathrm{dy}}(t)\right)\right)^2\end{array}} \quad (1)$$

$$\varepsilon_{\mathrm{mix}}(t) = \frac{e_{\mathrm{mix}}(t)}{\delta_0} \quad (2)$$

$$\theta_{\mathrm{mix}}(t) = \tan^{-1}\left(\frac{e_{\mathrm{st}}\sin\theta_{\mathrm{st}} + e_{\mathrm{dy}}(t)\sin\left(\theta_{\mathrm{dy}}(t)\right)}{e_{\mathrm{st}}\cos\theta_{\mathrm{st}} + e_{\mathrm{dy}}(t)\cos\left(\theta_{\mathrm{dy}}(t)\right)}\right) \quad (3)$$

where $\varepsilon_{\mathrm{mix}}$ is the relative mixed eccentricity, and e_{st} and e_{dy} are the amplitudes of the static and dynamic eccentricity, respectively. Their direction angles are presented as θ_{st} and θ_{dy}, respectively.

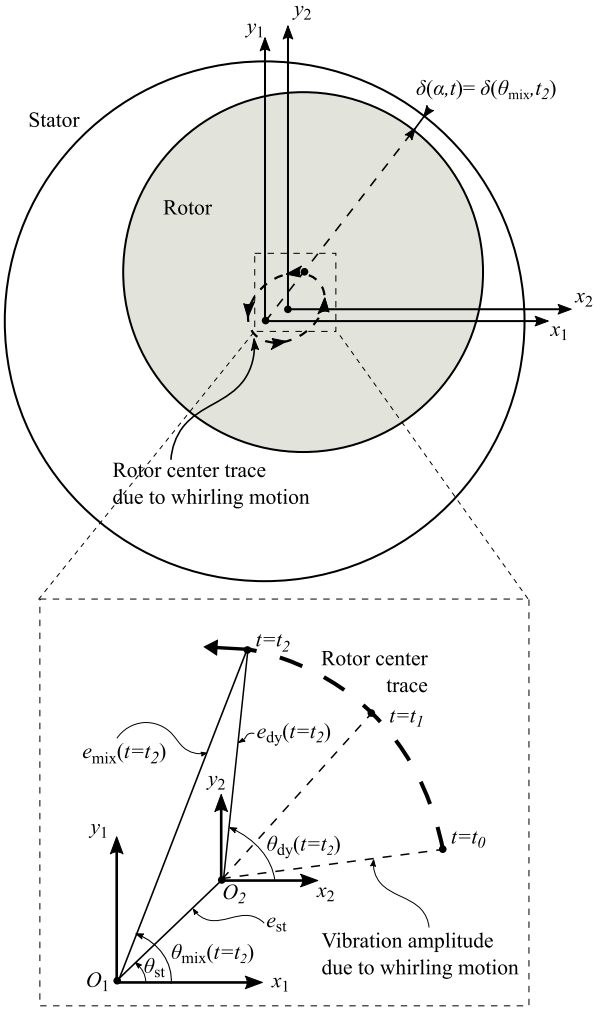

FIGURE 1. Concept of the mixed rotor eccentricity model based on time-step simulation.

B. UMP FORCE AND STIFFNESS MODEL

The UMP force is calculated by integrating the Maxwell stress tensor in the air-gap between the stator and the rotor. The Maxwell stress tensor is calculated from the air-gap magnetic flux density distribution. Therefore, the main task is to obtain accurate magnetic flux density distribution in the eccentric air-gap condition. However, its calculation is more complicated in an induction machine than in other machine types, such as permanent magnet machines. The reason for this is that the induction machine has a secondary magnetic circuit, where the rotor magnetic flux must be calculated, and its effect on the stator magnetic flux must be considered. However, in a situation where the slip is constant, the magnetizing current is nearly constant under variation in eccentricity and rotational speed [11], and therefore, a simple analytical model with magnetizing current instead of both the stator and rotor currents can be used to obtain the air-gap magnetic flux density distribution [12]. Thus, the magnetic flux density distribution in the eccentric air-gap condition is obtained by multiplication of MMF and air-gap permeance as in (4). Here, the MMF includes magnetizing current, and the air-gap permeance is based on the mixed eccentricity model.

$$\begin{aligned} &B_\delta(\alpha, t) \\ &= \frac{3\sqrt{2}\mu_0 N I_m}{\pi p \delta_0 \sqrt{1-\varepsilon_{\mathrm{mix}}(t)^2}} \\ &\times \left[1+2\sum_{m=0}^{\infty}\left(\frac{1-\sqrt{1-\varepsilon_{\mathrm{mix}}(t)^2}}{\varepsilon_{\mathrm{mix}}(t)}\right)^m \cos\left\{m\left(\alpha-\theta_{\mathrm{mix}}(t)\right)\right\}\right] \\ &\times \left[\begin{array}{l} w_{f1}\sin(\omega t - p\alpha) + \frac{w_{f5}}{5}\sin(\omega t + 5p\alpha) \\ +\frac{w_{f7}}{7}\sin(\omega t - 7p\alpha) + \cdots \end{array}\right] \end{aligned} \quad (4)$$

where α is a variable to define the angular position of the air-gap, μ_0 is the permeability of vacuum, N is the number of turns in a winding, I_{m} is the magnetizing current, p is the pole pair number, ω is the stator supply angular velocity, and $w_{f\nu}$ ($\nu = 1, -5, 7, \ldots$) is the winding factor. Thus, the UMP force is calculated by integrating the Maxwell stress tensor in the air- gap around the rotor surface as

$$\begin{aligned} F_{\mathrm{ump},x} &= \int_0^{2\pi} \frac{(B_\delta(\alpha,t))^2}{2\mu_0} r l_{\mathrm{st}} \cos\alpha d\alpha \\ F_{\mathrm{ump},y} &= \int_0^{2\pi} \frac{(B_\delta(\alpha,t))^2}{2\mu_0} r l_{\mathrm{st}} \sin\alpha d\alpha \end{aligned} \quad (5)$$

where r is the air-gap radius and l_{st} is the stator stack length.

With the established UMP force equation, the UMP stiffnesses in the horizontal and vertical directions are linearized around the static eccentricity point (x_{st}, y_{st}) as

$$k_{\mathrm{ump},x} \approx -\left.\frac{dF_{\mathrm{ump},x}}{dx}\right|_{x=x_{\mathrm{st}}}, k_{\mathrm{ump},y} \approx -\left.\frac{dF_{\mathrm{ump},y}}{dy}\right|_{y=y_{\mathrm{st}}}. \quad (6)$$

This analytical model has, however, a limitation related to the accuracy of the result. The model does not include the effects caused by variation in slip, slot opening, magnetic saturation, and flux leakages. Therefore, to overcome this limitation, these effects are incorporated into the model with the newly defined correction factor using the FEA results. The process to obtain the correction factor is as follows. First, a time-stepping FEA is conducted to calculate the UMP force in the static condition of the rotor eccentricity. Here, the FEA cases are selected based on variations of slip and eccentricity

in dynamic operation of the machine. Then, the correction factor is defined using the concept compensating the analytically calculated UMP force by increasing the mean air-gap in the analytical formula, in other words, decreasing the relative eccentricity. This factor is calculated inversely from the analytical formula using the UMP results calculated by the FEA. As the FEA results are obtained for the cases of variation in slip and eccentricity, the correction factor is a function of slip s and eccentricity, which is obtained using the curve fitting method for the digitized FEA results. Consequently, the mean air-gap is updated by multiplying the correction factor c as

$$\delta_0' = c\,(s, \varepsilon) \cdot \delta_0 \tag{7}$$

and then, the original analytical formula is updated using the updated mean air-gap. In this process, the change in the analytically calculated UMP caused by variation in slip and eccentricity is matched with the change in the FEA results in the same condition of variation in slip and eccentricity. Therefore, the accuracy of the updated analytical model depends on the accuracy of the FEA results and the cases calculated by the FEA.

III. ELECTRIC MACHINE OF THE CASE STUDY

For the case study, a two-pole high-speed induction generator was selected as a test machine. The generator was designed as a steam turbogenerator for a waste heat recovery system [13]. The main parameters of the machine are presented in Table 1, and its concept is shown in Fig. 2. The test machine has turbine and electric generator parts, and it is installed vertically on a support frame with vibration isolators. The machine has a vertical rotor supported by AMBs; the rotor has a squirrel cage electrical part between two radial bearings. The concept of the rotor–bearing system is shown in Fig. 3. Specifically, as the rotor is supported by AMBs, it is possible to adjust the target location of the rotor control within the gap of the touchdown bearing. It means that the static eccentricity condition can be controlled experimentally. Therefore, this test machine can be suitable for determining the UMP effects caused by variation in static eccentricity.

TABLE 1. Parameters of the induction generator under study.

Parameters (Unit)	Values
Rated electric power, kW	1000
Rated speed, RPM	12500
Rated voltage, V	390 / 675
Rated torque, N·m	766
Rated slip	0.00158
Rated stator current, A	1170
Magnetizing inductance, mH	0.835
Leakage inductance, mH	0.109
Number of pole pairs	1
Stack length, mm	380
Rotor outer diameter, mm	237
Mean air-gap length (radial), mm	5
Number of rotor bars	20
Air-gap length of touchdown bearing, μm	350
AMB stiffness, N/m	3.66×10^5 (ND[a]), 5.81×10^5 (D[a])
AMB damping, N·s/m	2100 (ND), 3332 (D)

[a] D = Drive side, ND = Non-drive side

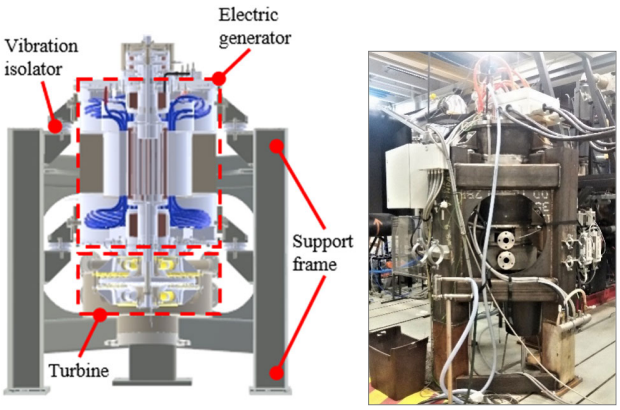

a) Concept of the test machine b) Prototype

FIGURE 2. Test machine (steam turbogenerator).

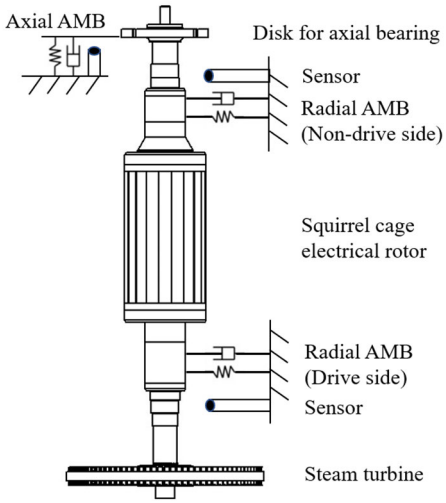

FIGURE 3. Concept of the rotor system supported by AMBs.

IV. IDENTIFICATION OF ROTOR–BEARING MODEL

To include the UMP effects in the rotordynamics simulation, the UMP model is incorporated into the equation of motion for the rotor–bearing system as an external nonlinear force as

$$\mathbf{M}\ddot{\mathbf{q}} + (\mathbf{C} + \Omega\mathbf{G})\dot{\mathbf{q}} + \mathbf{K}\mathbf{q} = \mathbf{F}_{\text{ub}} + \mathbf{F}_{\text{ump}} \tag{8}$$

where $\mathbf{q}$ is the displacement vector, and $\mathbf{M}$, $\mathbf{C}$, $\mathbf{G}$, and $\mathbf{K}$ are the mass, damping, gyroscopic, and stiffness matrices, respectively. The term Ω is the rotor angular velocity, and $\mathbf{F}_{\text{ub}}$, and $\mathbf{F}_{\text{ump}}$ denote the unbalance force, and the UMP force vectors, respectively.

The rotor–bearing system model of the test machine is established using the beam finite-element-based flexible rotor model and the simplified AMB model. First, the beam element model of the rotor is built as shown in Fig. 4. In this model, to simplify the calculation, the end ring, the turbine

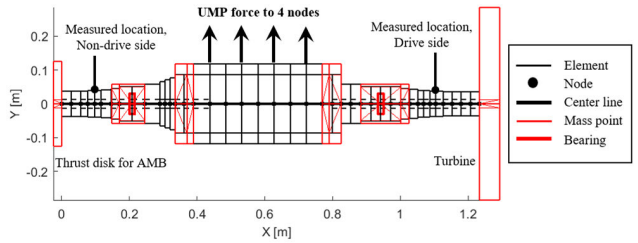

FIGURE 4. Beam finite element model of the rotor including UMP force.

impeller, and the disk of the axial AMB are modeled as rigid bodies. The model has four degrees of freedom per node, and it is assumed that there is no displacement in the axial direction and no rotation around the rotor axis as this study focuses only on the lateral vibration analysis. The rotor model is updated and validated by matching the mass, center of mass, and inertia properties with the reference parameters taken from a detailed CAD model.

Second, the simplified AMB model consisting of linearized constant coefficient spring and damper elements is connected between the rotor node and the ground. According to the initial estimation of the UMP effect, the effect is significant close to the rotor rigid body whirling mode, and therefore, the rigid rotor modes are selected to be used for AMB coefficient identification. It has a clear benefit in the bearing coefficient identification because the rotor itself does not contribute to the overall rotor–bearing system stiffness or dissipative damping. The AMB coefficient identification is accomplished in two steps. First, the bearing stiffness is tuned to match the simulated and measured cylindrical forward whirling mode frequencies of the supported rotor. Then, in the second part, the bearing damping coefficient is identified. In this process, instead of calculating the modal damping ratio based on measured data, the damping coefficient is adjusted to make the simulated vibration responses as similar as possible to the measured vibration responses in all the cases with and without UMP. Specifically, the process focuses on the combined trend of UMP effects rather than only the vibration amplitudes because there are still several uncertainties in the experimental results, such as the error in the static eccentricity setup and unidentified vibration caused by the AMB control. For the simulation of vibration responses, the exact residual unbalance identified during the rotor balancing process is incorporated into the numerical model. The residual unbalance is measured in two planes.

After the rigid rotor properties have been validated, the flexible mode frequencies of the unsupported rotor (i.e., free-free modes) are verified based on the experimental modal analysis.

The flexible frame model is excluded from the rotordynamics model for two reasons: first, there are no frame resonance modes within the operational speed range or right after the nominal operational speed, and second, the frame is supported on a stiff support by vibration isolators. The experimental modal measurement results obtained for the complete machine with the support equipped with vibration isolators verify that the dynamic stiffness of the frame is high enough to be excluded from the rotordynamics model.

Finally, the UMP force is applied to four nodes of the electric active part of the rotor model. Here, the UMP force at each node is calculated depending on the eccentricity at the node.

V. ANALYSIS OF UMP IN TEST MACHINE

To simulate the UMP effects on rotordynamics of the test machine, the air-gap magnetic flux density distribution and UMP are calculated using the developed method. Specifically, the time-variant characteristics of the UMP force and stiffness are investigated as they are strongly related to the UMP effect on rotordynamics. In the analysis of the time-variant UMP, the eccentricity condition is not changed in the time variation, that is, only static eccentricity is considered, because in the developed UMP model, dynamic eccentricity can be considered only through the rotordynamics simulation process, which obtains the rotor position at every time-step.

A. EFFECT OF CORRECTION FACTOR IN THE AIR-GAP FLUX DENSITY

To obtain the magnetic flux density distribution, the magnetizing current is calculated. In this analysis, however, instead of the well-known analytical approach [14], the magnetizing current is obtained from the phase current data (257 A) measured during the experiment, because this study focuses on the identification and experimental verification of UMP effects. Then, the flux density distribution is calculated using (4). To obtain an accurate UMP force equation, UMP forces calculated by the FEA and correction factors in six different eccentric conditions are obtained as shown in Table 2. Here, the correction factor c is inversely calculated to match the analytically calculated UMP force with the UMP force calculated by the FEA. To verify the effect of the correction factor, its effect on the MMF and the air-gap permeance are shown in Fig. 5, respectively. Because the correction factor changes the mean air-gap, the average and peak-to-peak amplitudes of the air-gap permeance decrease. However, the MMF is not changed. Consequently, the resulting air-gap flux density distributions are obtained as shown in Fig. 6. It can be seen that the distribution using the analytical model is close to the distribution calculated by the FEA when using the correction factor. In conclusion, it is found that when a correction factor is not included in the model, the amplitude of the magnetic flux density is much higher than the result from the FEA. The reason for this is that the effects of the slot opening, magnetic saturation, and leakage decrease the magnetic flux, but these effects are not included in the pure analytical model. The correction factor improves the UMP force by changing the air-gap permeance. When the correction factor increases, the static and dynamic terms of the air-gap permeance decrease simultaneously. This, in turn, has an impact on the flux density waveform. Finally, Table 2 shows the

TABLE 2. FEA-calculated UMP and correction factor.

Static eccentricity [%]	FEA-calculated UMP force [N]	Correction factor, c
1.5	48.1	1.812
3	96.3	1.816
6	192.9	1.817
10	323.3	1.817
15	489.5	1.816
20	663.2	1.812

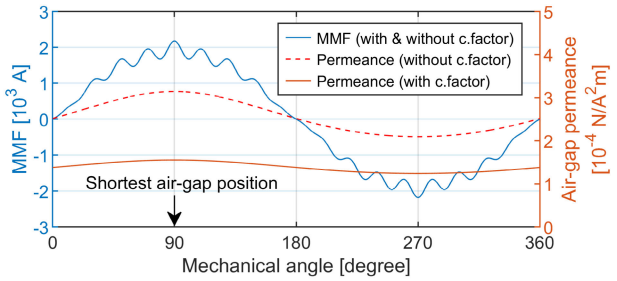

FIGURE 5. Effect of the correction factor (1.82) on the MMF and air-gap permeance in the 20% eccentricity condition.

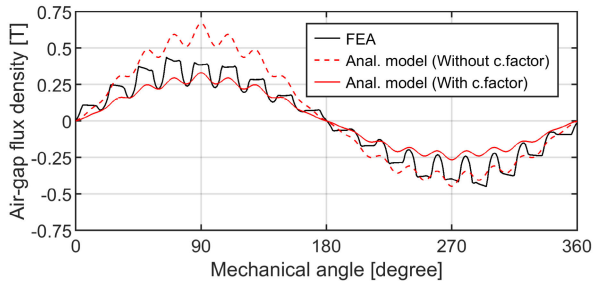

FIGURE 6. Effect of the correction factor (1.82) on the air-gap magnetic flux density distribution in the 20% eccentricity condition.

variation of the calculated correction factor when the static eccentricity varies from 0% to 20%. Its variation is below 0.3%. Thus, in this test machine, if the eccentricity is smaller than 20%, it is reasonable to use a constant correction factor (1.82) for efficient calculation.

B. TIME-VARIANT UMP

To investigate the time-variant characteristics of the UMP, the UMP force and stiffness in variation of static eccentricity and time are calculated as in Fig. 7. Here, time variation can be considered a variation in phase difference between the MMF and the air-gap permeance in Fig. 5, because this difference is the only time-dependent term to change the UMP in the static eccentricity condition. In this analysis, the stator supply frequency is set at 2 Hz, and the static eccentricity varies from 0% to 20%. The results show that the periodic fluctuation of the UMP occurs when time varies, and this periodic wave has a frequency of 4 Hz, which is twice the stator supply frequency. When the static eccentricity increases, the peak-to-peak amplitude of the UMP wave increases nearly linearly. Consequently, the UMP can excite the rotor with twice the stator supply frequency when static eccentricity is present, and this excitation force is amplified when the static eccentricity increases. However, the effect of static eccentricity on the linearized UMP stiffness is not significant. It means that the effect of static eccentricity on the negative stiffness of the UMP that changes the rotor natural frequency will be not significant. These characteristics of the UMP will be introduced again to interpret the UMP effects in the rotordynamics results.

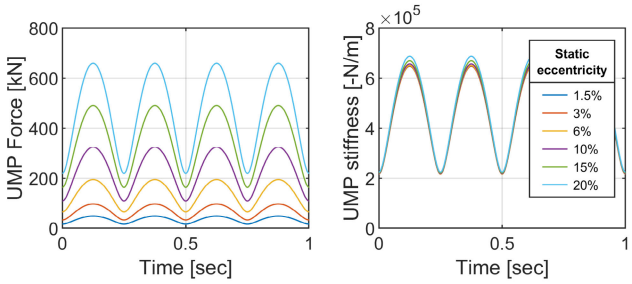

FIGURE 7. Time-variant characteristic of the UMP force and stiffness in six different eccentricities.

VI. UMP EFFECTS ON ROTORDYNAMICS

A. SIMULATION PLAN

Because the UMP force is nonlinear, a rotordynamics simulation based on time-step analysis is designed. Initially, natural frequencies and their modes are studied in the non-UMP condition using an eigenvalue analysis for determining the rotordynamic characteristics of the test machine. Then, an analysis to study the response caused by the mass unbalance and the UMP force is designed. To investigate the UMP effect in detail, the UMP force is divided into the UMP caused by static eccentricity and the UMP caused by dynamic eccentricity. The UMP caused by dynamic eccentricity results from the whirling motion of the rotor, and therefore, its effect can be determined by comparing the response result in the condition including UMP at the 0% static eccentricity with the result in the condition without UMP. The effect of the UMP caused by static eccentricity can be determined by comparing the response results in the conditions including UMP with different static eccentricities. Therefore, the response simulation is conducted for four cases: without UMP and with UMP for three different static eccentricity conditions (0%, 1.5%, and 2.25%).

B. EXPERIMENT PLAN FOR VERIFICATION

To determine the UMP effects experimentally and verify the simulation results, the experiment must demonstrate two conditions. First, the dynamic behavior of the rotor, not including UMP, must be measured. The test generator is designed to be operated by a steam turbine. However, it would require a mobile steam generator, which is not considered practical for the test. Hence, the machine is operated in the motor mode, and thus, the rotating condition excluding the UMP could be demonstrated only by turning off the motor at a higher speed

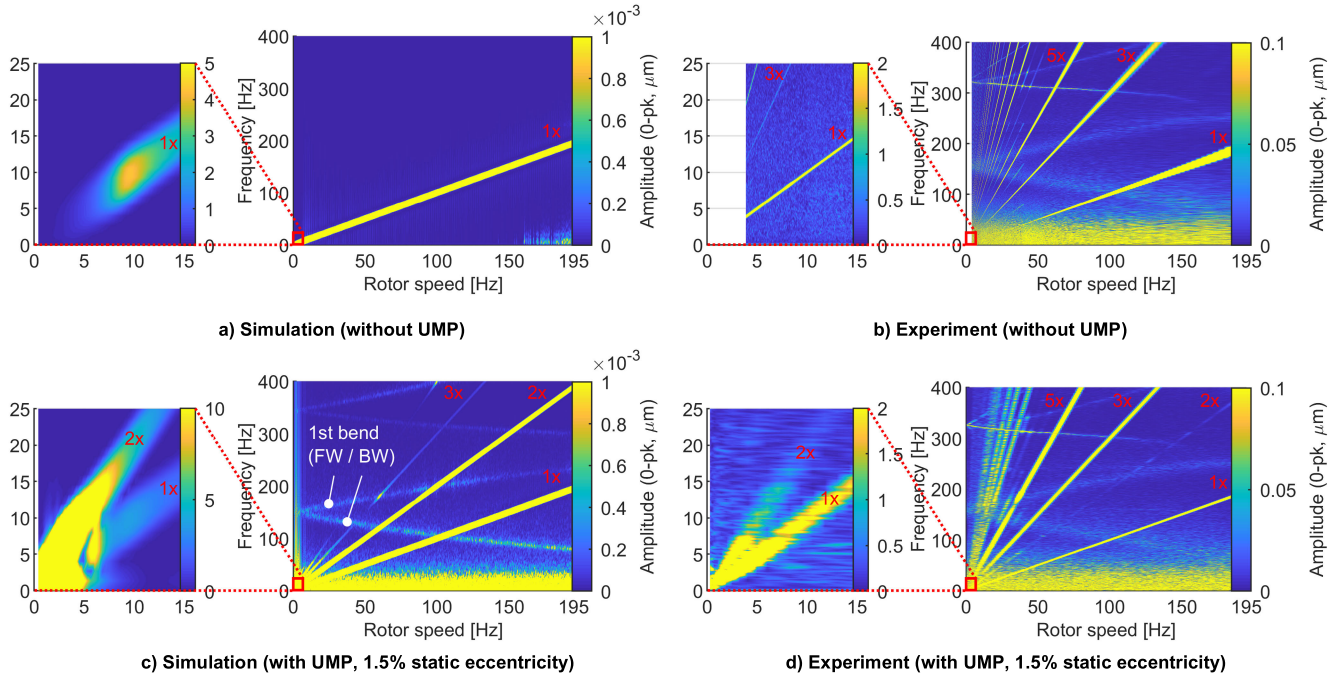

FIGURE 8. Comparison between simulation and experiment results of the forced vibration response in the radial direction of the drive-side bearing location.

and measuring the rotor vibration during the speed-down of the rotor. In the motor-off condition, deceleration of the rotor speed cannot be controlled, and it is lower when the speed decreases. Therefore, it was not possible to obtain measurement results in the same deceleration speed condition in two different UMP conditions: without and with UMP.

Secondly, different static eccentricity conditions must be demonstrated experimentally. The static eccentricity results from a deviation between the bearing center and the stator center. Therefore, in the test machine, the static eccentricity condition is simulated by changing the bearing center, which can be defined as the target location of the rotor center controlled by the AMBs. In this machine, accurate control of the bearing center can be achieved by using an AMB control, and therefore, three different static eccentricity conditions are demonstrated: 0%, 1.5% (75 μm), and 2.25% (125 μm) eccentricity. Here, the maximum possible eccentricity is limited by the air-gap (350 μm) of the touchdown bearing. On the other hand, there is one limitation on the setup of static eccentricity. In the test machine, initial misalignment between the stator and the bearing center is unavoidable, but it was not checked and assumed zero. Therefore, the actual static eccentricity has a difference with the value setup in the experiment, and it is not possible to perfectly demonstrate the 0% static eccentricity condition.

In order to determine the UMP effect on the rotor natural frequencies and vibrational amplitude versus rotor speed, the test machine runs down from 195 Hz to 0 Hz. In the process of the AMB control, unbalance force rejection control (UFRC) is carried out to minimize the unbalance response, but in the low speed range below 40 Hz, this control starts to destabilize the rotor because of the specific characteristics of the controller algorithm, and therefore, the UFRC is not used below the 40 Hz speed. Moreover, to identify the rotor natural frequency clearly in the measurement results, a random noise force is generated by the AMB to excite the rotor. The same process of experiments is repeated for four different cases: without UMP (Motor-Off) and with UMP (Motor-On) in static eccentricity conditions of 0%, 1.5%, and 2.25%.

C. ROTORDYNAMICS RESULTS INCLUDING UMP EFFECTS

Fig. 8 shows the spectral maps during ramp-down operation from the 195 Hz rotor speed in the simulation and the experiment. Changes in the rotor natural frequencies and additional vibration components are mainly investigated to determine the UMP effects. First, from these maps, the natural frequencies of the forward (FW) and backward whirling (BW) modes of the flexible rotor can be identified. When comparing the results without and with UMP, the results show that the natural frequencies of the flexible body whirling modes are practically not changed at all by the UMP. However, the rigid mode natural frequencies are not identified, and therefore, their change cannot be investigated by using these maps. Second, not only the synchronous vibration components but also additional harmonics are shown in the maps except for the simulation case not including the UMP. The 3rd- and 5th-order harmonics occur in both experiment cases: without and with UMP. These harmonics probably result from the AMBs [15]. When including the UMP, the 2nd harmonic occurs again, confirming that it is caused by the UMP. This effect is shown clearly when investigating the close-up map in the low speed

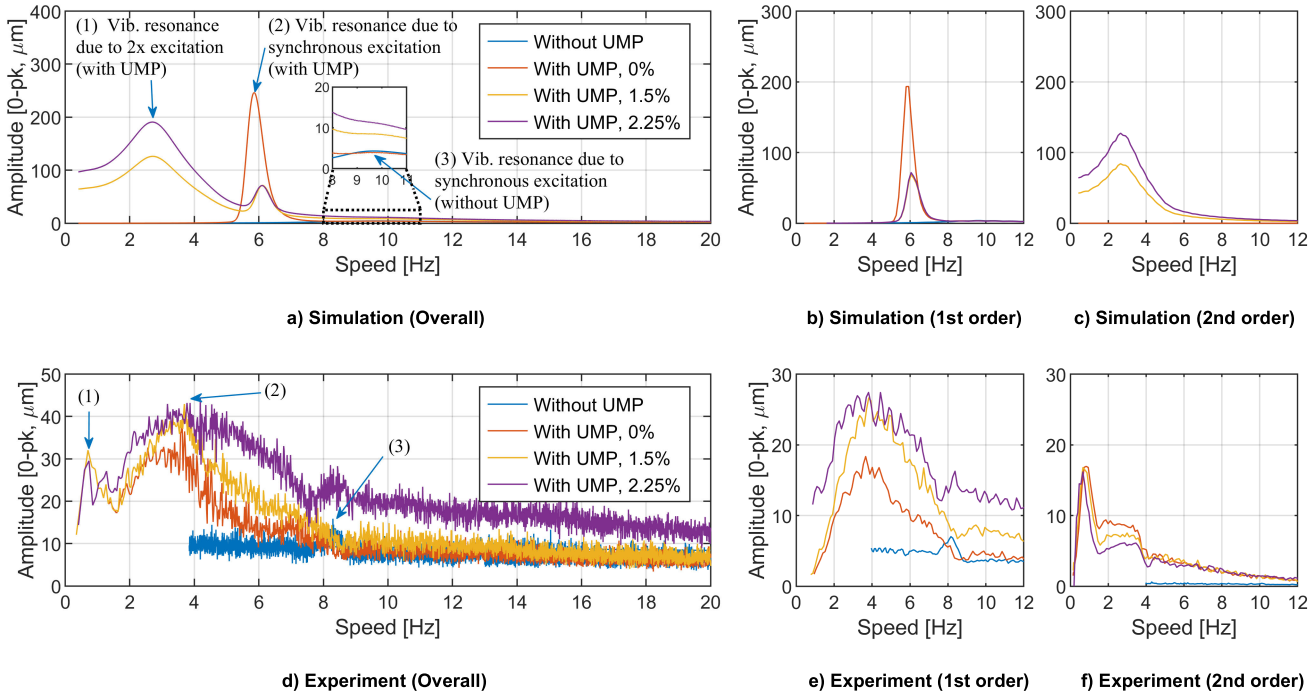

FIGURE 9. Comparison between simulation and experiment results of forced vibration response in the radial direction of the drive-side bearing location focused on the low speed range.

range. The magnitude of the 2nd-order harmonic is amplified when it coincides with the rigid mode natural frequency. This effect is shown in both the simulation and the experiment.

To investigate the UMP effect accurately in the change in the rigid mode frequency and the corresponding amplitude, the vibration responses below the 20 Hz rotor speed are shown in Fig. 9 with the overall amplitude. Moreover, the 1st-order and 2nd-order components are separated from the overall component to investigate the excitation cause of overall vibration. Figs. 9 (a) and (d) show the overall amplitudes measured at the drive-side bearing for four different cases. Here, two vibration resonances occur. One resonance comes from the synchronous excitation at the rigid mode natural frequency. The frequency of this resonance decreases when including the UMP effect. The other resonance occurs only in the case including the UMP caused by static eccentricity. This resonance, in turn, comes from the 2nd-order excitation amplified when coinciding with the rigid mode frequency. This interpretation is verified by the results of the 1st- and 2nd-order amplitude in Fig. 9. Thus, the first effect of the UMP is that the rigid mode natural frequency decreases from 8 Hz to 4 Hz in the experiment and from 9 Hz to 5 Hz in the simulation, and moreover, the corresponding vibration amplitude increases significantly. On the other hand, the effect of the static eccentricity in the natural frequency is not significant, and according to the simulation result, the static eccentricity decreases the vibration amplitude at the rigid mode natural frequency. This is probably due to the fact that when the static eccentricity is zero, the direction of the UMP force always coincides with the direction of the unbalance force, and therefore, the UMP force is used to amplify the synchronous vibration. However, when the amplitude of the static eccentricity becomes higher than that of the dynamic eccentricity, the direction of the UMP force is always toward the direction of the static eccentricity, and therefore, its effect on synchronous vibration is attenuated.

The second effect of the UMP is that the additional vibration caused by the 2nd-order excitation is generated. It is related to the characteristics of the time-variant UMP presented in section V. *B*. In the test machine, the 2nd-order excitation has the same frequency with twice the supply frequency excitation because the pole pair number of the test machine is one. According to the simulation results, the 2nd-order component occurs only when static eccentricity is present, and it is amplified when its frequency coincides with natural frequencies. Moreover, the peak amplitude increases when the static eccentricity increases. The UMP effect caused by static eccentricity is shown in the experiment with the same trend, but the effect caused by the increase in static eccentricity is shown differently in the experiment. When the static eccentricity increases, the experiment shows that the peak vibration amplitude caused by synchronous excitation increases. On the other hand, the peak vibration amplitude caused by the 2nd-order excitation decreases. Interestingly, this trend is exactly the opposite to the simulation results. It is most likely caused by the uncertainty related to the eccentricity in the experimental setup. Moreover, a perfect condition for the 0% static eccentricity cannot be demonstrated in the experimental setup. However, if the actual static eccentricities are assumed to have opposite values to the setup

values, these opposite results can be a strong evidence of the UMP effects in vibration excited by the synchronous and 2^{nd}-order (twice the stator supply frequency) components caused by static eccentricity.

VII. CONCLUSION

In this paper, an analysis and experimental verification method for determining the UMP effects on the rotordynamics of induction machines were presented. Using the developed UMP model, the time-variant characteristics of the UMP were analyzed. Finally, the UMP effects on rotordynamics were investigated using both simulation and experimental methods. The main results of this study can be summarized as follows:

1) The analysis results of the UMP force and stiffness show that the UMP force has periodic excitation characteristics with twice the stator supply frequency when static eccentricity is present. Correspondingly, the amplitude of the excitation increases when the static eccentricity increases. The UMP stiffness, however, is not changed significantly by static eccentricity.
2) The results on rotordynamics show that the UMP reduces the rigid mode natural frequency of the rotor system. This reduction is mainly caused by dynamic eccentricity. The effect of static eccentricity is not significant. This is probably due to the fact that the effect of static eccentricity on the UMP stiffness is not significant.
3) The results on rotordynamics show that the UMP generates twice the stator supply frequency vibration. This vibration results mainly from static eccentricity. Most likely, the reason for this is that when static eccentricity is present, the time-variant UMP force excites the rotor with twice the stator supply frequency.
4) A trend of the UMP effects on rotordynamics is shown clearly in both simulation and experiment. It confirms that the process developed for rotordynamics simulation considering the UMP effect has a good accuracy and computation efficiency.
5) The experimental setup has a limitation with respect to the inaccuracy in determining the actual static eccentricity. In the future experiment work, these limitations can be overcome by finding a method to measure the original static eccentricity in the assembly process of the machine.

REFERENCES

[1] X. Xu, Q. Han, and F. Chu, "Review of electromagnetic vibration in electrical machines," *Energies*, vol. 11, no. 7, p. 1779, Jul. 2018.
[2] D. G. Dorrell, "Sources and characteristics of unbalanced magnetic pull in three-phase cage induction motors with axial-varying rotor eccentricity," *IEEE Trans. Ind. Appl.*, vol. 47, no. 1, pp. 12–24, Jan. 2011.
[3] H. Chuan and J. K. H. Shek, "Calculation of unbalanced magnetic pull in induction machines through empirical method," *IET Electr. Power Appl.*, vol. 12, no. 9, pp. 1233–1239, Nov. 2018.
[4] T. P. Holopainen, A. Tenhunen, and A. Arkkio, "Electromechanical interaction in rotordynamics of cage induction motors," *J. Sound Vib.*, vol. 284, nos. 3–5, pp. 733–755, Jun. 2005.
[5] H. Kim, A. Posa, J. Nerg, J. Heikkinen, and J. T. Sopanen, "Analysis of electromagnetic excitations in an integrated centrifugal pump and permanent magnet synchronous motor," *IEEE Trans. Energy Convers.*, vol. 34, no. 4, pp. 1759–1768, Dec. 2019.
[6] H. Kim, J. Nerg, T. Choudhury, and J. T. Sopanen, "Rotordynamic simulation method of induction motors including the effects of unbalanced magnetic pull," *IEEE Access*, vol. 8, pp. 21631–21643, 2020.
[7] D. G. Dorrell and O. Kayani, "Measurement and calculation of unbalanced magnetic pull in wound rotor induction machine," *IEEE Trans. Magn.*, vol. 50, no. 11, pp. 1–4, Nov. 2014.
[8] Z. Q. Zhu, D. Ishak, D. Howe, and J. Chen, "Unbalanced magnetic forces in permanent-magnet brushless machines with diametrically asymmetric phase windings," *IEEE Trans. Ind. Appl.*, vol. 43, no. 6, pp. 1544–1553, 2007.
[9] A. Arkkio, M. Antila, K. Pokki, A. Simon, and E. Lantto, "Electromagnetic force on a whirling cage rotor," *IEE Proc.-Electr. Power Appl.*, vol. 147, no. 5, pp. 353–360, Sep. 2000.
[10] P. Pennacchi, "Computational model for calculating the dynamical behaviour of generators caused by unbalanced magnetic pull and experimental validation," *J. Sound Vib.*, vol. 312, nos. 1–2, pp. 332–353, Apr. 2008.
[11] J. Nerg, J. Pyrhonen, and J. Partanen, "Finite element modeling of the magnetizing inductance of an induction motor as a function of torque," *IEEE Trans. Magn.*, vol. 40, no. 4, pp. 2047–2049, Jul. 2004.
[12] M. Berman, "On the reduction of magnetic pull in Induction motor with off center rotor," in *Proc. IEEE Ind. Appl. Conf. 28th IAS Annu. Meeting*, Oct. 1993, pp. 343–350.
[13] A. Grönman, J. Nerg, E. Sikanen, T. Sillanpää, N. Nevaranta, E. Scherman, A. Uusitalo, N. Uzhegov, A. Smirnov, J. Honkatukia, P. Sallinen, R. P. Jastrzebski, J. Heikkinen, J. Backman, J. Pyrhönen, O. Pyrhönen, J. Sopanen, and T. Turunen-Saaresti, "Design and verification of a hermetic high-speed turbogenerator concept for biomass and waste heat recovery applications," *Energy Convers. Manage.*, vol. 225, Dec. 2020, Art. no. 113427.
[14] J. Pyrhönen, T. Jokinen, and V. Hrabovcova, *Design of Rotating Electrical Machines*, 2nd ed. Hoboken, NJ, USA: Wiley, 2014.
[15] X. Xu, S. Chen, and J. Liu, "Elimination of harmonic force and torque in active magnetic bearing systems with repetitive control and notch filters," *Sensors*, vol. 17, no. 4, p. 763, Apr. 2017.

HEESOO KIM was born in Seoul, South Korea, in 1979. He received the B.S. and M.S. degrees in mechanical engineering from Hanyang University, Seoul, in 2005 and 2007, respectively. He is currently pursuing the Ph.D. degree with the Department of Mechanical Engineering, LUT University, Lappeenranta, Finland. After graduation, he worked as a Turbocharger Development Engineer for marine and vehicle engines. His research interests include rotordynamics for electrical machines, specifically study about electromechanical interaction from air-gap eccentricity, stator deformation, and other geometric non-idealities.

EERIK SIKANEN received the M.Sc. degree in mechanical engineering and the D.Sc. (technology) degree from LUT University, Lappeenranta, Finland, in 2014 and 2018, respectively. He is currently working as a Postdoctoral Researcher with the Laboratory of Machine Dynamics, LUT. His research interests are high-speed rotor dynamics analysis and general vibration dynamics of rotating machinery. He is mainly concentrating on three-dimensional solid finite element modeling of high-speed machinery and systems including contact and thermomechanical effects.

JANNE NERG (Senior Member, IEEE) received the M.Sc. degree in electrical engineering, the Licentiate of Science (technology) degree, and the D.Sc. (technology) degree from LUT University, Lappeenranta, Finland, in 1996, 1998, and 2000, respectively. He is currently an Associate Professor with the Department of Electrical Engineering, LUT University. His research interests are in the field of electrical machines and drives, especially electromagnetic and thermal modeling and design of electromagnetic devices.

TEEMU SILLANPÄÄ (Member, IEEE) received the B.Sc. and M.Sc. degrees in electrical engineering from LUT University, Lappeenranta, Finland, in 2012 and 2013, respectively, where he is currently pursuing the Ph.D. degree with the Control Engineering and Digital Systems Laboratory. His research interests include control systems, digital signal processing, and power electronic circuits related to active magnetic bearing suspended high-speed electrical machines.

JUSSI T. SOPANEN (Member, IEEE) was born in Enonkoski, Finland, in 1974. He received the M.Sc. degree in mechanical engineering and the D.Sc. (technology) degree from LUT University, Lappeenranta, Finland, in 1999 and 2004, respectively. He has been a Researcher with the Department of Mechanical Engineering, LUT University, from 1999 to 2006. He has also worked as a Product Development Engineer in electric machine manufacturer Rotatek Finland Ltd., from 2004 to 2005. From 2006 to 2012, he worked as a Principal Lecturer in mechanical engineering and research manager in the Faculty of Technology, Saimaa University of Applied Sciences, Lappeenranta, Finland. He is currently serving as a Professor in machine dynamics with LUT University. His research interests are rotor dynamics, multi-body dynamics, and mechanical design of electrical machines.